Grid Interactive Charging Control for Plug-in Electric Vehicles

R. J. Rei, F. J. Soares, *Student Member*, *IEEE,* P. M. Rocha Almeida, *Student Member*, *IEEE,* J. A. Peças Lopes, *Senior Member*, *IEEE*

***Abstract*—This paper describes technical solutions to be adopted by Electric Vehicles (EV) battery grid interfaces in order to get the provision of ancillary services to the grid. The developed solution exploits a load battery charge control approach based in local fast grid cooperative response to frequency or voltage deviations. In a scenario characterized by a massive deployment of EV, the adoption of such a solution allows an improvement on the power system dynamic behaviour, namely in small island grids or MicroGrids operated in islanded mode.**

***Index Terms*—Charging Management, Droop Control, Electric Vehicle, Improved Power Quality Converters, MicroGrid.**

I. Introduction

OVER half of the world's oil consumption is nowadays allocated to the transportation sector, and a large portion of it is used by road vehicles. Despite the predictable depletion of fossil fuel reserves, the oil consumption has increased over time, as well as the related CO2 emissions, being of utmost importance to implement measures to break this cycle. Given these circumstances the change towards an electricity mobility paradigm is becoming more and more needed, given that this shift will bring clear advantages for cities air quality and for the global warming problematic [1].

At first look, taking an Electric Vehicle (EV) as a simple load during battery charge, it would represent a large amount of electric power consumed, approaching in some cases the power of a typical domestic household at peak load. From the distribution grid point of view, it is clear that the direct effects of massive integration of EV will provoke a substantial increase on electric energy demand and will raise load values at peak hours. Additionally, as the majority of the distribution grid at the Low Voltage level (LV) have a considerably high R/X ratio and are operated using a radial configuration, some problems are likely to appear with the deployment of EV: the lines around the feeding points tend to reach high congestion levels, while electrically farthest buses have a tendency to face voltage drops, losses might increase and voltage unbalances can also occur [1].

The easiest way of solving the above presented problems is to make large investments to reinforce the grid's infrastructures in order to allow EV owners to charge their vehicles at free will. However this will make EV to be seen as a "threat" by Distribution System Operators (DSO), who want to avoid these investments at all cost.

In order to break up with these technical/economic barriers, advanced management and control strategies must be implemented for EV charging. This way, instead of being a burden for the grid, EV will act as an active element in the network, capable of helping in the control of the grid operating conditions. While the increase on the electric energy consumption at peak hours can be easily tackled merely by shifting the EV charging towards the valley hours, there are other problems whose resolution demands the implementation of higher complexity strategies.

In the situations where the above stated strategy is insufficient to solve a given problem, like high branches' congestion levels or abnormal voltage profiles, a bolder approach involving advanced management and control concepts must be employed. Nevertheless, the successful implementation of these approaches relies on the existence in the grid of some fundamental elements, like EV/grid interfaces and a suitable communication platform.

The MicroGrid (MG) concept involves the presence of a communication infrastructure, providing in this way the technical environment for the implementation of the advanced management and control concepts developed for EV. The MG hierarchical management structure comprises two levels with complementary functionalities that are performed by two different elements: a MicroGrid Central Controller (MGCC), which heads the control structure, and local controllers who are responsible for managing the existent loads and micro-generation units [2], [3]. By adding some extra features to the MGCC and a new element to the MG concept, the Vehicle Controller (VC), it will be easy to make the MGCC able to control also the EV charging. This way EV batteries may be faced as dynamic loads (able to vary its charging rate), and in an even bolder generalization they can be exploited as storage devices with the capability

This work was supported in part by Fundação para a Ciência e Tecnologia under Grants SFRH/BD/48491/2008 and SFRH/BD/47973/2008 and within the framework of the Project with the Reference MIT-Pt/SES-GI/0008/2008.

The authors are with Instituto de Engenharia de Sistemas e Computadores do Porto (INESC Porto) and Faculdade de Engenharia da Universidade do Porto (FEUP), Porto, Portugal (e-mails: rjrei@inescporto.pt, fsoares@inescporto.pt; pedro.almeida@fe.up.pt, jpl@fe.up.pt;).

of injecting power into the grid, i.e. featuring Vehicle-to-Grid (V2G). Each VC works jointly with a power electronic converter interface between EV batteries and the grid. Given this new reality, the MGCC could be seen as a LV vehicle aggregator who can collect information about the EV willing to provide system services and sell them in the electricity market. The envisaged synergetic approach between EV and MG will not only improve the MG operating conditions but also increase the number of electric vehicles that can be safely integrated into distribution networks.

In several studies, the detailed models of power electronic converters were replaced by simpler dynamic models based on their control functions, as these are more adequate when the main goal is to perform macro scale studies with a large number of power electronic converters operating simultaneously. However, the practical feasibility of the lower detail models must be confirmed from the viewpoint of the power electronic converter control. To do so, first of all, suitable electronic converter architecture must be chosen, as well as a proper control approach, in order to achieve satisfactory converter stability, robustness, and power quality specifications. In this stage, a transient analysis focused on the converter detailed model representation should be done, in order not to undervalue commutation inherent side effects, like harmonic distortion, displacement factor and response delays.

Afterwards, upper control layers, based in the frequency or voltage deviations, should be applied to the converter/battery system. The overall performance of such an approach can be evaluated by integrating the detailed control model in a small islanded grid and analysing its dynamic behaviour when load variations occur.

This work describes the detailed control solution developed for the EV battery grid interface and includes a technical feasibility study of the power electronic converter control for grid islanded operation modes. All the simulations were performed using the software Matlab/Simulink.

II. Power Electronic Converter Selection

Power electronic converters are designed to efficiently interface electric systems with different voltage, current and frequency needs. Regarding EV, the power converter will manage the energy flow between the distribution grid and the battery, so each side requirements will be used as guidelines in the converter selection process.

A. Grid Interface

As a first approach to the problem, this work considers a three-phase grid connection, instead of a single-phase. This solution contributes to avoid voltage unbalances by reducing phase currents, as EV charging at its nominal rate represents a large amount of power being absorbed from the grid. It is assumed that the converter will connect to a three-phase 400V, 50 Hz grid with standard power quality requirements.

B. Battery Interface

Among the major types of chemistries, Li-ion appears to be the election battery type for the PHEV and EV expected to be in the markets in a near future [4]. Nevertheless, due to the lack of detailed information about Li-ion batteries, it was chosen for this study a NIMH chemistry type, as these batteries are currently used in some hybrid electric vehicles and much information about it is already available. The battery pack model used in this study is based in the Toyota Prius NHW11, which includes 38 modules of 6 Panasonic HHR650D cells, with 6.5 Ah and 1.2 V each, all of them in series, resulting in total 273.6 V and 1778 Wh (the largest of the Prius packs).

The NIMH battery model was included in the simulation platform using the SymPowerSystem block. The Simulink battery model was presented and validated in [5], using data available on HHR650D cells. Model limitations like related to ageing or temperature effects, don´t have relevant impact on the objectives of this work.

The main concern of the charging system, on top of any grid requirements, is to preserve the EV battery life, implying that recommended charge methods must be followed imperatively. Hence, the battery charger should always superimpose the suitable charging rates and other constraints defined by the manufacturer over the orders sent by the charging management system. The most important specifications provided by the NIMH battery manufacturer are the following:

--Standard charging: 0.1 C (0.65 A), requiring 16 hours;

--Fast charging: 1 C (6.5 A), requiring 1.2 hours (ranging from 0,5 C to 1 C is possible);

--Fast charge transition restoration current: current is limited within 0.2 C to 0.3 C and cell voltage is below 0.8 V;

--Trickle charging current: 0.033 C to 0.05 C might be applied after rapid charge or in deeply discharge conditions.

Several timers for each charging stage and stop charge triggering events (like maximum voltage cell), were also defined (temperature related events were not taken into account, as previously mentioned) [6], [7].

C. Power Electronic Converter

The chosen converter should be an AC/DC current controlled charger circuit, with a topology that allows the bidirectional power flow between the grid and the EV. From the battery point of view, the converter should charge at a controlled constant current, thus small current ripple will be desirable. From the grid point of view the converter must be a three-phase device, presenting phase currents with low Total Harmonic Distortion (THD) and close to unity displacement factor. Thus, the selection of an Improved Power Quality Converter (IPQC) is the better option. The IPQC converters use solid-state switching devices like insulated gate bipolar transistors (IGBT) and reactive elements like inductors in the AC side and capacitors in the DC side (helping to limit AC currents and DC voltages ripples). Hence, to achieve the mentioned specifications, a bidirectional three-phase and three-level diode clamped converter topology was adopted [8], [12]. This circuit can be seen as a boost converter and so, looking toward the grid nominal voltage and the battery voltage working range, a step-down three-phase transformer was used in the grid connection side, providing also galvanic insulation.

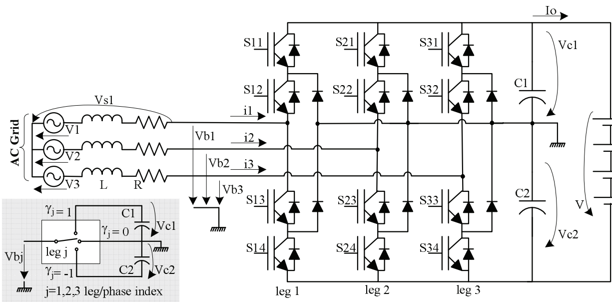

Fig. 1. Three-phase three-level diode clamped converter with IGBT Sji. C1=C2=10 mF and L=8 mH.

In Fig. 1 the Vj voltages sources are the secondary y-y step-down transformer voltages. Each converter leg can be emulated by a three position switch as shown in the grey zone. Therefore, Vbj voltages can assume three different values available from the capacitor divider. Those three level voltages implicitly reduce the input currents distortions, which is the main advantage of this converter. In the next equations γ_j is the switch function for converter leg j:

$$Vb_j = \begin{cases} Vc_1 & \text{se } \gamma_j = 1 \;\Leftrightarrow S_{j1}, S_{j2}\ \text{ON} \wedge S_{j3}, S_{j4}\ \text{OFF} \\ 0 & \text{se } \gamma_j = 0 \;\Leftrightarrow S_{j2}, S_{j3}\ \text{ON} \wedge S_{j1}, S_{j4}\ \text{OFF}, \quad j = 1,2,3 \\ -Vc_2 & \text{se } \gamma_j = -1 \Leftrightarrow S_{j3}, S_{j4}\ \text{ON} \wedge S_{j1}, S_{j2}\ \text{OFF} \end{cases} \tag{1}$$

$$Vb_j = \underbrace{\frac{\gamma_j}{2}\left(\gamma_j + 1\right)}_{\Gamma_{1j} \in \{0;1\}} Vc_1 + \underbrace{\frac{\gamma_j}{2}\left(1 - \gamma_j\right)}_{\Gamma_{2j} \in \{-1;0\}} Vc_2 = \Gamma_{1j}\, Vc_1 + \Gamma_{2j}\, Vc_2 \tag{2}$$

III. CONVERTER CONTROL

The converter will be controlled in current mode. To act in the output current of the battery, an internal AC current control loop and an external DC current control loop are used, as shown in the Fig. 2.

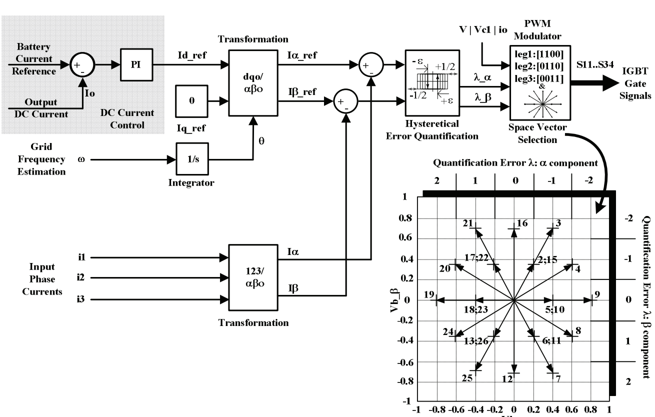

Fig. 2. AC and DC (grey area) currents controls/representation of Vbj voltages in αβ frame and vector selection strategy.

A. AC Current Control

Nonlinear and time variant structures, like power converters, restrain the use of linear control strategies and, for that, using sliding mode control is appropriate.

By using the dq rotating reference frame (with grid angular velocity input), the balanced symmetrical three-phase set of AC input currents can be represented for a null quadrature projection (as unity displacement factor is required). The output of the DC control loop is the reference for the direct current on the dq frame that will control the amplitude of AC currents phasors. The grid frequency estimation was done using the zero-crossing method described in [9].

As aforementioned, each Vbj voltage can assume three different discrete values, so $3^3 = 27$ combinations for Vbj are possible. Assuming that the capacitor voltages are equalized, Vc1 = Vc2 = V/2, Vbj possible values can be referred to V as -½, 0 and ½. Then an ab0/αβ0 transformation can be applied to the voltage vectors [Vb1; Vb2; Vb3], resulting in 27 different vectors in the αβ space. Doing the necessary transformations to the αβ0 frame, α and β errors between references and measured AC currents can be computed. The represented Vbj vectors define five different values in β axis and nine different values in α axis. However, when selecting a single α or β value, a maximum of five different values are defined in the orthogonal component. Hence, current errors can be quantified by means of a sum of four hysteretic comparators output (λ_α and λ_β) with maximum and minimum saturation levels of -½ and ½ (thus, outputting -2, -1, 0, 1 and 2). The dead-band of each comparator is centred in zero and has a width of ε,1.1×ε, 1.2×ε and 1.3×ε (ε is the bigger error considered as zero). The ε parameter (related to the ripple of the AC currents) reduction is limited by the maximum switch frequency of the IGBT.

Considering a sliding surface defined as $S(e_{i\_\alpha,\beta},t) = k(i_{\alpha,\beta\_ref} - i_{\alpha,\beta}) = 0$, finite switching frequency will imply $S(e_{i\_\alpha,\beta},t) \neq 0$, so there's a certain dynamic error tending to zero, resulting in AC currents ripple. To assure the stability of the system under sliding mode control, sliding mode existence and reaching conditions must be fulfilled. The latter establishes that enough command action (Vbj value) must be available, in order to handle perturbation effects, while the former establishes that in sliding mode $S(e_i,t)\dot{S}(e_i,t) < 0$ (if $S(e_i,t) > 0 \rightarrow \dot{S}(e_i,t) < 0$, $S(e_i,t)$ will decrease to zero; if $S(e_i,t) < 0 \rightarrow \dot{S}(e_i,t) > 0$, $S(e_i,t)$ will increase to zero) [10]. Applying the last condition, if $S(e_i,t) > 0$, $i_{\alpha,\beta}$ must increase:

$$\left(\frac{d\, i_{\alpha,\beta\, ref}}{dt} - \frac{d\, i_{\alpha,\beta}}{dt}\right) < 0 \Leftrightarrow \frac{d\, i_{\alpha,\beta}}{dt} > 0 \tag{3}$$

Thus, according to the Fig. 1 definitions, a vector with negative value $V_{\gamma,\beta}$ must be applied. Reciprocal logic can be applied to $S(e_{i\_\alpha,\beta},t) < 0$, resulting in a choice of vector with positive $V_{\gamma,\beta}$ value. According to the error quantification [λ_α, λ_β] the vectors can be selected as shown in Fig. 2.

However for some error arrangements, no vector seems suitable (for [-2,-2] the nearest vector is the 3, and this vector will be selected also for [-1,-2]). A consequence of applying a sliding mode control is variable switching frequency, because switching occurs at the needed moment.

As shown in Fig. 2, univocal vector selection is not always possible (e.g. both 13 and 26 vectors can be selected for error [1, 1]) and the resulting degree of freedom can be used for capacitors equalization, as can be concluded from (4).

$$\frac{dVc_k}{dt} = \frac{\Gamma_{k1}\, i_1 + \Gamma_{k2}\, i_2 + \Gamma_{k3}\, i_3}{C_k} - \frac{I_o}{C_k}, \text{ k is the capacitor index} \quad (4)$$

Vector 26 has $\Gamma_1 = (0, 0, 0)$ and if $Io > 0$ then $dVc1/dt < 0$ and capacitor C1 discharges; vector 13 has $\Gamma_2 = (0, 0, 0)$ and if $Io > 0$ then $dVc2/dt < 0$ and capacitor C2 discharges. Each of the 27 represented vectors in $\alpha\beta$ space correspond to a unique combination of the three γ_j switching functions, so vectors can be translated in ON/OFF signals for IGBT gates.

B. DC Current Control

The application of the 123/dq0 transformation to equation (4) parameters, results in the following expression for C1:

$$\frac{dVc_1}{dt} = \frac{\Gamma_{1d}}{C_1} id - \frac{I_o}{C_1}, \text{ with } \begin{array}{l} \Gamma_{1d} = \Gamma_{1\alpha} \cdot \cos(\theta) + \Gamma_{1\beta} \cdot \sin(\theta) \\ \Gamma_{1\alpha} = 2/3 \cdot (\Gamma_{11} - 1/2 \cdot \Gamma_{12} - 1/2 \cdot \Gamma_{13}) \\ \Gamma_{1\beta} = 2/3 \cdot (-\sqrt{3}/2 \cdot \Gamma_{12} + \sqrt{3}/2 \cdot \Gamma_{13}) \end{array} \quad (5)$$

By using the sliding mode control, AC currents follow the reference values with some delay (Td), related to switching frequency,

$$id(s) = id\_ref(s) \cdot e^{-sTd} \xrightarrow[\exp\ Taylor\ Series]{1^{st}\ Order\ Term} id(s) = 1/(1 + s \cdot Td) \cdot id\_ref(s) \quad (6)$$

The voltage output dynamic can be neglected when compared to the dynamic of the currents and, if so, expression (5) is simplified to $I_o = \Gamma_{1d} \times i_d$. Additionally, assuming an unity displacement factor (i_q=0) and that converter losses are neglected, the input and output powers are the same and equal to $V \times I_o = V_d \times i_d$, where V_d is the direct component of the three-phase input voltages. Therefore, a simplified model for the converter controlled in current mode is presented in Fig. 3.

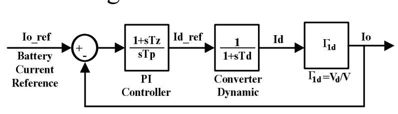

Fig. 3. DC current control loop with simplified converter.

In order to obtain a zero static error, integral action is needed, thus a PI controller was selected. The zero of this controller was selected in order to cancel the high frequency pole, which is related to the dynamics of the converter AC currents. Therefore $T_z = T_d = 1/(2\pi f_s)$, where f_s is the switching frequency. Finally, a manual fine-tuning of PI parameters was performed.

IV. Grid Interactive Charging Management

In order to improve the local grid dynamic behaviour in islanding mode the EV charging process must respond to frequency and voltage variations. Frequency is an instantaneous indication of the power balance, so if the frequency drops, it will be desirable to decrease the charging rate of connected EV (reverse observation is valid, mutatis mutandis). EV load reduction will also help to correct eventual voltage sags that might appear in the system when a considerable number of EV is charging simultaneously.

The EV charging current as a function of the grid frequency/voltage deviations, will then assume a proportional nature with positive slopes outside a dead-band centred at nominal frequency/voltage and saturating at the considered absolute maximum and minimum values. This kind of proportional control is called “droop control” [11], [12]. Fig. 4 presents an example for frequency and voltage droop. For this case, the dead-band was defined symmetrically around the nominal frequency/voltage and, within this range, the charging rate is kept constant and equal to a set-point value, so the autonomous control is immune to frequency/voltage variations inside this window. Droop saturation maximum (1 C) and minimum (0) must be defined to occur, respectively, above and below the grid admissible maximum and minimum frequency/voltage values. The slopes of this control approach became intrinsically defined with the characterisation of the dead-band, charging rate set-point and saturation values.

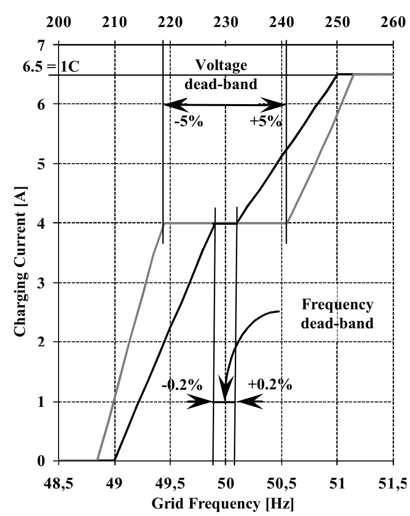

Fig. 4. Frequency and voltage droops: definition of dead-bands and set-point of 4A for the charging rate

Under this approach, the charging rate of EV will result from the merging effects of both frequency and voltage droops. Despite slight propagation effects, frequency is a global scope variable, as any deviation is simultaneously and equally transmitted to all points of the grid. On the other hand, voltage is a local variable which is very dependent on local load profiles. So, for a particular EV charging control, local voltage conditions will always prevail over frequency variations, given that voltage can only be corrected by EV connected locally while frequency problems might be solved with the contribution of any EV connected to the system.

The behaviour of the EV charger controller will be defined according to a signal received from the MGCC or other hierarchically above control entities. If a so a named “voltage droop priority signal” is 1, the EV will react only to voltage variations. Otherwise if that signal is 0 and measured voltage is inside its droop dead-band, frequency droop control is responsive to frequency deviations.

In conclusion, the EV charging controller can react locally and autonomously to frequency and voltage measurements, based in the defined droops, or to signals received periodically from grid upper hierarchical control levels (Fig. 5), based in previous collected inputs (like batteries SOC, user defined period of charge and expected SOC at the hour of disconnection, etc).

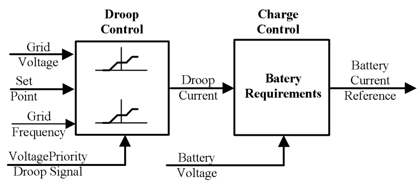

Fig. 5. “Droop Control” block outputs will be subject to constraints imposed by the “Charge Control”. The DC current control reference is the main output.

V. Simulation Model and Results

The evaluation of the performance of the described control and management strategies is tested in a small islanded grid represented in Fig.6.

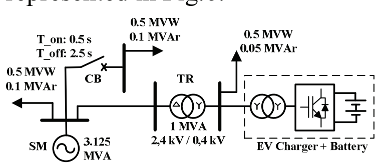

Fig. 6. Grid model used for EV charger test.

The grid has a single synchronous machine generator with its own PI controller, in order to perform primary and secondary frequency control; the machine has also voltage regulation. The circuit-breaker CB will switch on a load with considerable value. CB switch on and switch off events occur at 0.5 s and 2.5 s, respectively.

A. Constant Rate Charging

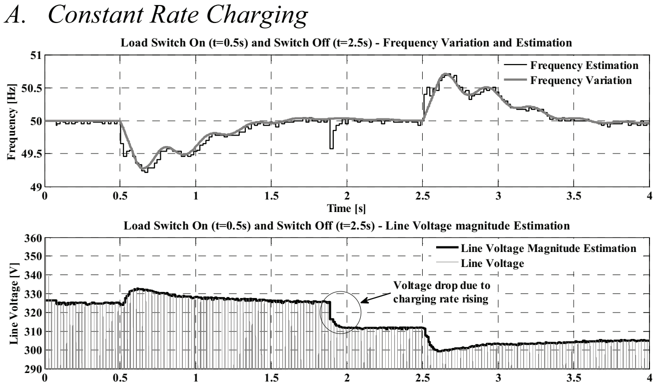

Fig. 7. Frequency and voltage grid values and respective measurements.

For this set of simulations, constant 6.5 A = 1C rapid charging current is imposed to the battery pack, with 2.45% SOC, in order to point out the action of the charger control in assuring the battery requirements. Other basic control goals defined above will also be checked. The related effects of the CB switching events are shown in Fig. 7.

The voltage drop near 1.9 s of simulation time occurs, not as consequence of any CB switching events, but as a result of the charging rate increase reported in Fig. 8.

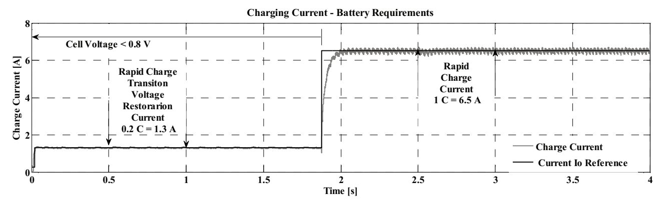

Fig. 8. Charger Control action to meet battery charge rate requirements.

The upstream reference for the charging current is set to 6.5 A, however, the charge controller only outputs this value when SOC increases so that the cell voltage rises above 0.8 V. Until that, reduced current is applied (rapid charge transition voltage restoration current). A fast step response without oscillations was obtained, thus pointing to a good dynamic response. Steady state error is negligible and the charging current presents small ripple. Thus, good tracking behaviour is obtained and immunity to voltage and frequency disturbances is verified.

In Fig. 9 are represented the waveforms of the line currents in the grid side of the converter transformer. The currents have a sinusoidal shape, with a frequency of 50 Hz, and form a three-phase symmetric and balanced system. Small currents switching ripple results from the high switching frequency combined with filtering effect of the line inductors. Thus, currents THD values are below the 5% grid standard limit. The second graph of Fig. 9 shows a tiny or absent displacement angle, that results in a close to unity displacement factor (the converter behaves almost like a resistive variable load).

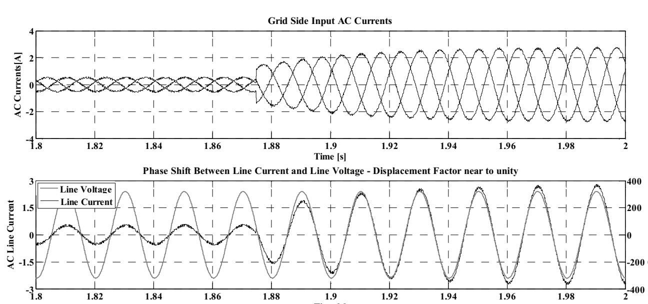

Fig. 9. Three phase currents and phase shift.

B. Grid Interactive Charging Management

For this set of simulations, battery pack SOC was set in 10%, thus the battery charge controller doesn’t restrain the upstream current reference output from the frequency droop control presented in Fig. 4. Voltage droop was disabled by means of setting the droop nominal voltage far from the grid nominal voltage.

As shown in Fig. 10, after a transient initial overshoot, the charge current tracks, with delay of tens of ms, the frequency variation according above mentioned frequency droop. The charging rate is immune to frequency variations within the defined dead-band. Data cross-checking between Fig. 11 and Fig. 4 provide also consistent results (e.g. for 49.5 Hz, a near to 2A charging current is obtained, while for 50.5 Hz it is obtained 5A).

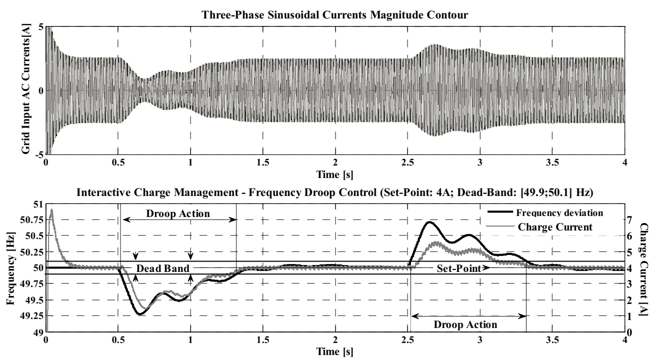

Fig. 10. Frequency droop control – charging rate and resulting AC currents.

The magnitude of AC currents is shaped according to the charging current values.

In Fig. 11 it is depicted the default behaviour of the control management, using both frequency and voltage droops. So when the measured voltage is within its droop dead-band, the frequency droop control is active and can react to frequency deviations. Otherwise, only voltage droop is active, reacting to eventual voltage variations.

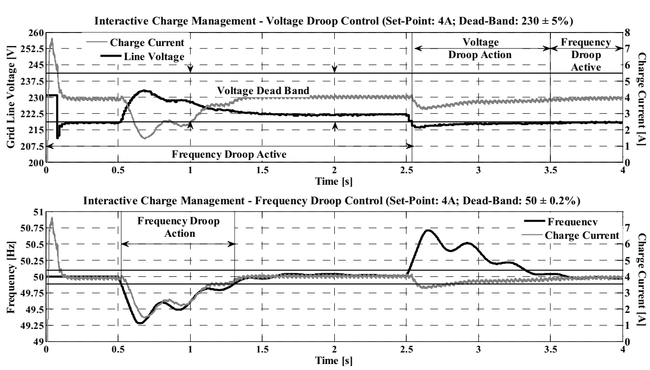

Fig. 11. Frequency and voltage droops action – Frequency droop enabled.

If the voltage droop priority signal is 1, only the voltage droop is enabled, as shown in Fig. 12, after 2.5 s.

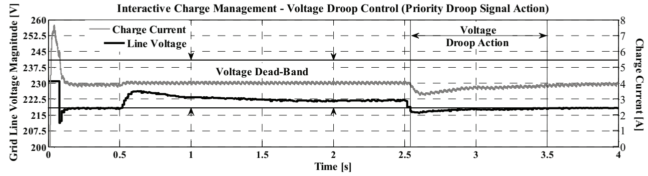

Fig. 12. Frequency and voltage droops action – Frequency droop disabled.

VI. Conclusion

In this paper, the technical feasibility of mentioned EV charging management strategies is confirmed by means of electronic power converter selection and application of proper control techniques. Besides the single application of the frequency droop, a method to handle the coexistence of voltage and frequency droops was also developed.

Currently, it is being developed a single-phase model to conduct simulations similar to those performed in this paper, as single-phase connections are much more common than three-phase ones.

In addition, the work being presently developed will not only contemplate EV load controllability, but also its capability to provide power to the grid (V2G concept). EV control strategies will be enhanced in order to improve EV potential to provide ancillary services to the grid [14].

References

[1] J. A. Peças Lopes, F. J. Soares, P. M. Rocha Almeida, Patrícia C. Baptista, Carla M. Silva, Tiago L. Farias, "Quantification of Technical Impacts and Environmental Benefits of Electric Vehicles Integration on Electricity Grids", *ELECTROMOTION 2009*, Lille, France, July, 2009.

[2] J. A. Peças Lopes, C. L. Moreira, A. G. Madureira, "Defining Control Strategies for MicroGrids Islanded Operation", *IEEE Transactions On Power Systems*, vol. 21, no. 2, May, 2006.

[3] J. A. Peças Lopes, C. L. Moreira and F. O. Resende, "MicroGrids black start and islanding operation", *Proc. 15th PSCC*, Belgium, 2005.

[4] F. Nemry, G. Leduc, A. Muñoz, "Plug-in Hybrid and Battery-Electric Vehicles: State of the research and development and comparative analysis of energy and cost efficiency", JRC Technical Notes - Annex I, October, 2009.

[5] Olivier Tremblay, Louis-A. Dessaint, Abdel-Illah Dekkiche, "A Generic Battery Model for the Dynamic Simulation of Hybrid Electric Vehicles", *Vehicle Power and Propulsion Conference*, Arlington, Texas, USA, 2007.

[6] Panasonic Nickel Metal Hydride Batteries Technical Handbook.

[7] Nickel Metal Hydride Batteries: Individual Datasheet HH650D.

[8] Bhim Singh, Brij N. Singh, Ambrish Chandra, Kamal Al-Haddad, Ashish Pandey, Dwarka P. Kothari, "A Review of Three-Phase Improved Power Quality AC-DC Converters", *IEEE Trans. Ind. Electron*, vol. 51, no. 3, 2004.

[9] V. Backmutsky, V. Zmudikov, "Accurate Frequency Estimation in Power Systems by DSP", *Proceedings of 18th IEEE Conference in Israel*, Tel-Aviv, Israel, May, 1995.

[10] Muhammad H. Rashid, "Power Electronics Handbook", *Academic Press*, 2nd ed., ch. 34, 2006, pp.955-993.

[11] J. A. Peças Lopes, P. M. Rocha Almeida, F. J. Soares, N. Hatziargyriou, "Electric Vehicles Grid Integration Under the MicroGrid Concept", Smart Grids and Mobility - Smart Grids and Mobility, Würzburg, Germany, June, 2009.

[12] J. A. Peças Lopes, Silvan A. Polenz, C. L. Moreira, Rachid Cherkaoui, "Identification of control and management strategies for LV unbalanced microgrids with plugged-in electric vehicles." *Electric Power Systems Research,* In Press.

[13] Sharanya Jaganathan, Wenzhong Gao, "Battery Charging Power Electronics Converter and Control for Plug-in Hybrid Electric Vehicle", *Vehicle Power and Propulsion Conference*, Michigan, USA, 2009.

[14] J. A. Peças Lopes, P. M. Rocha Almeida, F. J. Soares, "Using Vehicle-to-Grid to Maximize the Integration of Intermittent Renewable Energy Resources in Islanded Electric Grids", ICCEP 2009 - International Conference On Clean Electrical Power Renewable Energy Resources Impact, Capri, Italy, June, 2009.